New physics effects in $B \to K^{(*)}\nu\nu$ decays

C. S. Kim[*] and Yeong Gyun Kim[†]

Department of Physics, Yonsei University, Seoul 120-749, Korea

T. Morozumi[‡]

Department of Physics, Hiroshima University, 739-8526 Higashi-Hiroshima, Japan

We present a model-independent analysis of exclusive rare B decays, $B \to K^{(*)}\nu\nu$. The effect of possible new physics is written in terms of dimension-6 four-Fermi interactions. The lepton number violating scalar- and tensor-type interactions are included, and they induce $B \to K^{(*)}\nu\nu(\bar\nu\bar\nu)$ decays. We show systematically how the branching ratios and missing mass-squared spectrum depend on the coefficients of the four-Fermi interactions. [S0556-2821(99)00421-X]

PACS number(s): 13.20.He

I. INTRODUCTION

The flavor-changing-neutral-current (FCNC) process $b \to s\nu\bar\nu$ is a theoretically very clean mode in the standard model (SM) [1]. However, it might be extremely difficult to measure precisely the inclusive mode $B \to X_s\nu\bar\nu$ because it requires to reconstruct all X_s (together with two neutrinos). Experimentally it could be much easier to measure the exclusive modes $B \to K^{(*)}\nu\bar\nu$. The corresponding processes in K-meson system are $K_L \to \pi^0\nu\bar\nu$ and $K^+ \to \pi^+\nu\bar\nu$, and the expected branching ratios are 10^{-10} to 10^{-11} [1,2]. Compared with the rare decays of the K meson, the branching fractions of the B-meson decays are much larger, and the theoretical estimates are $\sim 10^{-5}$ for $B \to K^*\nu\bar\nu$ case and $\sim 10^{-6}$ for $B \to K\nu\bar\nu$ case [3,4]. The form factors of the decay process $K \to \pi\nu\bar\nu$ in the SM are related to the well known K_{l3} decay with isospin symmetry [1]. In the B system, while the form factors of $B \to \rho(\pi)\nu\bar\nu$ are directly related to those of $B \to \rho(\pi)l\nu$ decay, for $B \to K^{(*)}\nu\bar\nu$ processes they are only related to those of $B \to \rho(\pi)l\nu$ in the SU(3) limit [4]. Therefore, we still have to rely on models to estimate the form factors. Although this may introduce some model dependence of the hadronic form factors, it is still worth studying the exclusive decays $B \to K^{(*)}\nu\bar\nu$. Because of the higher statistics, we could study not only the branching fraction but also the distributions, such as missing mass-squared spectrum.

In this paper, we investigate the possible new physics effects on the branching ratio and the spectrum of $B \to K^{(*)}\nu\nu$ decays. The spectrum is sensitive to the types of the interactions and is useful for discriminating the various new physics effects [5]. We assume that the new physics effects are parametrized by dimension-6 four-Fermi interactions. (See Ref. [6] for the most general analysis of inclusive decays $B \to X_s l^+ l^-$.) Further, we assume that the right-handed component of (anti)neutrinos is supplied by charge

————————
[*]Email address: kim@kimcs.yonsei.ac.kr
[†]Email address: ygkim@cskim.yonsei.ac.kr
[‡]Email address: morozumi@theo.phys.sci.hiroshima-u.ac.jp

conjugated field of the left-handed neutrinos. In the SM, only one operator with the structure $(V-A)_{\text{quarks}} \times (V-A)_{\text{neutrinos}}$ contributes to the process. In extension of the SM, but still within chirality conserving four-Fermi interaction, another structure $(V+A)_{\text{quarks}} \times (V-A)_{\text{neutrinos}}$ is possible. Further, including the chirality changing interactions, the lepton number violating operators with the types $S_{\text{quarks}} \times S_{\text{neutrinos}}$ (S = scalar-type interactions) and $T_{\text{quarks}} \times T_{\text{neutrinos}}$ (T = tensor-type interactions) are also possible. The scalar and vector interactions were studied in the context of $K \to \pi\nu\bar\nu$ in a left-right model in Ref. [7].

Thus the most general model independent Lagrangian is given by

$$
\begin{aligned}
\mathcal{L} = \frac{\sqrt{2}G_F\alpha}{\pi}\Big\{&(C^V_{Lij}\overline{s_L}\gamma_\mu b_L + C^V_{Rij}\overline{s_R}\gamma_\mu b_R)(\overline{\nu_{Li}}\gamma^\mu\nu_{Lj}) \\
&+ (C^S_{Rij}\overline{s_L}b_R + C^S_{Lij}\overline{s_R}b_L)[\overline{(\nu_{Li})^C}\nu_{Lj}] \\
&+ (\widetilde{C}^S_{Rij}\overline{s_L}b_R + \widetilde{C}^S_{Lij}\overline{s_R}b_L)[\overline{\nu_{Li}}(\nu_{Lj})^C] \\
&+ C^T_{Lij}(\overline{s_R}\sigma_{\mu\nu}b_L)[\overline{(\nu_{Li})^C}\sigma^{\mu\nu}\nu_{Lj}] \\
&+ C^T_{Rij}(\overline{s_L}\sigma_{\mu\nu}b_R)[\overline{\nu_{Li}}\sigma^{\mu\nu}(\nu_{Lj})^C] + \text{H.c.}\Big\},
\end{aligned}
\tag{1}
$$

where the neutrino species are denoted by i,j. From Eq. (1), we note the following points: (i) C^V_L, C^V_R terms contribute to $B \to K\nu\bar\nu$ process, (ii) C^S_L, C^S_R, C^T_L terms contribute to $B \to K\bar\nu\bar\nu$ process, and (iii) $\widetilde{C}^S_L$, $\widetilde{C}^S_R$, C^T_R terms contribute to $B \to K\nu\nu$ process. In the Appendix, we derive the statistical factors for the production of (even theoretically) indistinguishable final state neutrinos, i.e., $B \to K^{(*)}\nu_i\nu_i$ and $B \to K^{(*)}\bar\nu_i\bar\nu_i$.

II. FORM FACTORS

First we write the form factors for $B \to K$ case as follows:

$$
\langle K(p')|\bar{s}\gamma_\mu b|\bar{B}(p)\rangle = f_+(p+p')_\mu + f_-(p-p')_\mu, \tag{2}
$$

TABLE I. Parameters of the fit $f_i(q^2)=f_i(0)/[1-\sigma_1 q^2+\sigma_2 q^4]$ to the $B\to(K,K^*)$ transition form factors in the GI-OGE model.

| Ref. | $f_+(0)$ | $f_-(0)$ | $s(0)$ | $g(0)$ | $f(0)$ | $a_+(0)$ | $a_-(0)$ | $h(0)$ | $g_+(0)$ | $g_-(0)$ |
| | σ_1 | σ_1 | σ_1 | σ_1 | σ_1 | σ_1 | σ_1 | σ_1 | σ_1 | σ_1 |
	σ_2	σ_2	σ_2	σ_2	σ_2	σ_2	σ_2	σ_2	σ_2	σ_2
GI-OGE	0.33	-0.27	0.057	0.063	2.01	-0.0454	0.053	0.0056	-0.3540	0.313
	0.0519	0.0524	0.0517	0.0523	0.0212	0.039	0.044	0.0657	0.0523	0.053
	0.00065	0.00066	0.00064	0.00066	0.00009	0.00004	0.00023	0.0010	0.0007	0.00067

$$\langle K(p')|\bar{s}\sigma_{\mu\nu}b|\bar{B}(p)\rangle=i\frac{f_T}{m_B}[(p+p')_\mu(p-p')_\nu$$
$$-(p-p')_\mu(p+p')_\nu]. \qquad (3)$$

From Eq. (2) the scalar form factor is obtained:

$$\langle K(p')|\bar{s}b|\bar{B}(p)\rangle=\frac{1}{m_b-m_s}[f_+(m_B^2-m_K^2)+f_-q^2]. \qquad (4)$$

In the rest frame of the B meson, $p=(m_B,0)$ and $p'=(\sqrt{\mathbf{p'}^2+m_K^2},\mathbf{p'})$, and

$$p+p'=(m_B+\sqrt{\mathbf{p'}^2+m_K^2},\mathbf{p'}),$$

$$q=p-p'=(m_B-\sqrt{\mathbf{p'}^2+m_K^2},-\mathbf{p'}). \qquad (5)$$

The matrix element of the tensor operator in the B-meson rest frame is given by

$$\langle K(p')|\bar{s}\sigma^{0i}b|\bar{B}(p)\rangle=-2ip'^i f_T, \qquad (6)$$

where all the other components are zero. Therefore, near the zero recoil the tensor form factor is suppressed by a factor of (p'/m_B) compared with that of the scalar operator. The form factors for $B\to K^*$ are written in the same way,

$$\langle K^*(p',\epsilon)|\bar{s}\gamma_\mu b|\bar{B}(p)\rangle=ig\epsilon_{\mu\nu\lambda\sigma}\epsilon^{*\nu}(p+p')^\lambda(p-p')^\sigma, \qquad (7)$$

$$\langle K^*(p',\epsilon)|\bar{s}\gamma_\mu\gamma_5 b|\bar{B}(p)\rangle=f\epsilon_\mu^*+a_+(\epsilon^*\cdot p)(p+p')_\mu$$
$$+a_-(\epsilon^*\cdot p)(p-p')_\mu, \qquad (8)$$

$$\langle K^*(p',\epsilon)|\bar{s}\sigma_{\mu\nu}b|\bar{B}(p)\rangle=g_+\epsilon_{\mu\nu\lambda\sigma}\epsilon^{*\lambda}(p+p')^\sigma$$
$$+g_-\epsilon_{\mu\nu\lambda\sigma}\epsilon^{*\lambda}(p-p')^\sigma$$
$$+h\epsilon_{\mu\nu\lambda\sigma}(p+p')^\lambda$$
$$\times(p-p')^\sigma(\epsilon^*\cdot p). \qquad (9)$$

From Eqs. (7),(8), we obtain the scalar and pseudoscalar form factors, respectively,

$$\langle K^*(p',\epsilon)|\bar{s}b|\bar{B}(p)\rangle=0, \qquad (10)$$

$$\langle K^*(p',\epsilon)|\bar{s}\gamma_5 b|\bar{B}(p)\rangle=\frac{-1}{m_b+m_s}[f(\epsilon^*\cdot p)+a_+(\epsilon^*\cdot p)$$
$$\times(m_B^2-m_{K*}^2)+a_-(\epsilon^*\cdot p)q^2]. \qquad (11)$$

For numerical calculations of the $B\to K,K^*$ transition form factors, we use a dispersion quark model calculation [8] in the whole kinematic range of q^2 with the parametrization

$$f_i(q^2)=\frac{f_i(0)}{1-\sigma_1 q^2+\sigma_2 q^4}.$$

In Ref. [8], the authors adopt the quark masses and the wave functions of the Godfrey-Isgur (GI) model [9] for the hadron spectrum with a switched-off one-gluon exchange (OGE) potential. It is found that the resulting form factors are in good agreement with the lattice simulations at large q^2. For convenience, we present the simple fit results of the GI-OGE model, $f_i(0)$, σ_1 and σ_2, in Table I.

III. MISSING MASS-SQUARED SPECTRUM AND BRANCHING RATIOS

Here we assume the mass of neutrinos to be zero, and therefore, we neglect possible effects of neutrino mass in the spectrum and the branching ratios. Now let us derive the missing mass-squared spectrum $d\Gamma/dq^2$. In this Section we show the results for the different flavor cases, i.e., $B\to K^{(*)}\nu^i\bar{\nu}^j$ ($i\neq j$), $B\to K^{(*)}\bar{\nu}^i\bar{\nu}^j$ ($i\neq j$), and $B\to K^{(*)}\nu^i\nu^j$ ($i\neq j$). For the cases $i=j$, we then get the following results. For $B\to K^{(*)}\nu\bar{\nu}$, the results are the same as the case with $i\neq j$. For $B\to K^{(*)}\nu\nu$ and $B\to K^{(*)}\bar{\nu}\bar{\nu}$, the results should be multiplied by the statistical factor two. The derivation of the statistical factors for the production of (theoretically) indistinguishable final state neutrinos is given in the Appendix.

We first study $B\to K$ case, and the missing mass-squared spectra are given as

$$\frac{d\Gamma(B\to K\nu\bar{\nu})}{dq^2}=\frac{G_F^2\alpha^2}{96\pi^5}|C_L^V+C_R^V|^2 f_+^2|p'|^3, \qquad (12)$$

$$\frac{d\Gamma(B\to K\nu\bar{\nu})}{dq^2}=\frac{G_F^2\alpha^2}{256\pi^5}|C_L^S+C_R^S|^2\frac{|p'|q^2}{m_B^2(m_b-m_s)^2}$$
$$\times[f_+(m_B^2-m_K^2)+f_-q^2]^2$$
$$+\frac{G_F^2\alpha^2}{48\pi^5}|C_L^T|^2\frac{f_T^2}{m_B^2}|p'|^3 q^2, \qquad (13)$$

$$\frac{d\Gamma(B \to K \nu \nu)}{dq^2} = \frac{G_F^2 \alpha^2}{256 \pi^5} |\tilde{C}_L^S + \tilde{C}_R^S|^2 \frac{|p'| q^2}{m_B^2 (m_b - m_s)^2}$$

$$\times [f_+(m_B^2 - m_K^2) + f_- q^2]^2$$

$$+ \frac{G_F^2 \alpha^2}{48 \pi^5} |C_R^T|^2 \frac{f_T^2}{m_B^2} |p'|^3 q^2, \qquad (14)$$

where $|\mathbf{p}'|$ is the three-momentum magnitude of K in the B-meson rest frame and can be written as

$$|\mathbf{p}'| = \frac{\sqrt{\lambda(m_B^2, m_K^2, q^2)}}{2 m_B}, \qquad (15)$$

where $\lambda(a,b,c) = a^2 + b^2 + c^2 - 2ab - 2bc - 2ca$. The flavor indices in C's are suppressed and should be read as $C_{Lij}^V = C_L^V$ ($i \neq j$), $C_{Rij}^V = C_R^V$ ($i \neq j$), $C_{Lij}^T = C_L^T$ ($i \neq j$), $C_{Rij}^T = C_R^T$ ($i \neq j$), $\tilde{C}_{Lij}^T = \tilde{C}_L^T$ ($i \neq j$), $\tilde{C}_{Rij}^T = \tilde{C}_R^T$ ($i \neq j$). Summing all three contributions, Eqs. (12)–(14), the total differential decay rate is given by

$$\frac{d\Gamma(B \to K)}{dq^2} = |C_L^V + C_R^V|^2 V_K(q^2)$$

$$+ (|C_L^S + C_R^S|^2 + |\tilde{C}_L^S + \tilde{C}_R^S|^2) S_K(q^2)$$

$$+ (|C_L^T|^2 + |C_R^T|^2) T_K(q^2), \qquad (16)$$

where

$$V_K(q^2) = \frac{G_F^2 \alpha^2}{96 \pi^5} f_+^2 |p'|^3, \qquad (17)$$

$$S_K(q^2) = \frac{G_F^2 \alpha^2}{256 \pi^5} \frac{|p'| q^2}{m_B^2 (m_b - m_s)^2}$$

$$\times (f_+(m_B^2 - m_K^2) + f_- q^2)^2, \qquad (18)$$

$$T_K(q^2) = \frac{G_F^2 \alpha^2}{48 \pi^5} \frac{f_T^2}{m_B^2} |p'|^3 q^2. \qquad (19)$$

The end points of the phase space, i.e., $q^2 = 0$ and $q^2 = (m_B - m_K)^2$, correspond to $|p'| = (m_B^2 - m_K^2)/(2 m_B)$ (maximal recoil) and $|\mathbf{p}'| = 0$ respectively (zero recoil). The characteristic dependence on the kinematical variables q^2 and $|p'|$ in Eqs. (17)–(19) can be seen in Fig. 1(a). $V_K(q^2)$, $S_K(q^2)$ and $T_K(q^2)$ correspond to the solid, dashed, and dotted line, respectively. Ignoring the momentum dependence of the form factors, near the minimum of the missing mass-squared, the spectrum due to tensor- and scalar-type interactions linearly grows as q^2 increases while the spectrum of vector-type interactions approaches a nonzero constant as $q^2 \to 0$. This is related to the fact that the collinear neutrino and antineutrino have zero total helicity while the collinear (anti)neutrino and (anti)neutrino have $-(+)1$ total helicity. At the maximum-recoil limit of the K meson, the conservation of the total helicity cannot be satisfied for the case of two neutrinos or two antineutrinos in the final states. Near
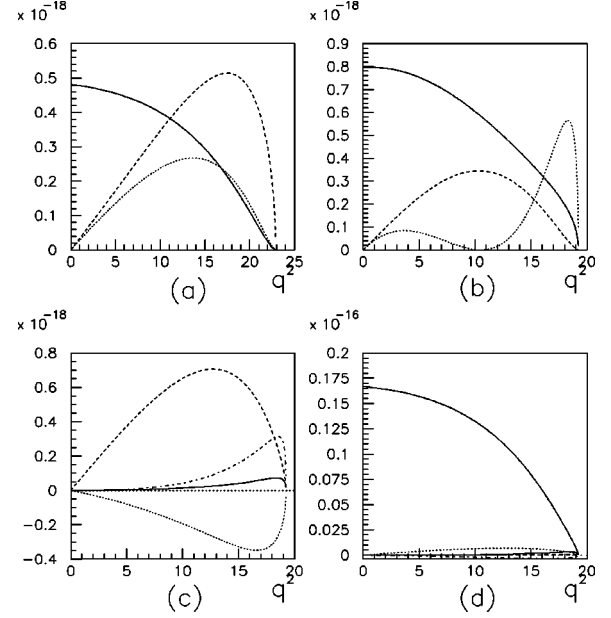

FIG. 1. q^2 (in GeV^2 scale) dependence of various factorized functions (in GeV^{-1} scale) for (a) $(B \to K)$, (b) $(B \to K^*)_L$, (c) and (d) $(B \to K^*)_T$. The functions are defined in Sec. III. See text for the details.

the end point of the spectrum, the first derivative of the spectrum due to the scalar interactions becomes infinity while that of the other spectra becomes zero. The sharp rise of the spectrum of the scalar interaction near the zero-recoil of K meson is related to the fact that the back-to-back (anti)neutrino and (anti)neutrino have zero total helicity. The suppression of the spectrum occurs for the vector interactions because the back-to-back antineutrino and neutrino have ± 1 helicities and the helicity conservation cannot be satisfied. As for the spectrum of the tensor interaction near the zero recoil, there is a suppression factor of $|\mathbf{p}'|^2$ compared with that of the scalar interaction.

We now turn to $B \to K^*$ case. By setting $\epsilon = \epsilon_L = (|\mathbf{p}'|, 0, 0, E_K)$ (longitudinal polarization), or $\epsilon = \epsilon_T$ (transverse polarization), we can show that the following matrix elements vanish:

$$\langle K^*(p', \epsilon_L) | \bar{s} \gamma_\mu b | \bar{B}(p) \rangle = 0,$$

$$\langle K^*(p', \epsilon_T) | \bar{s} \gamma_5 b | \bar{B}(p) \rangle = 0. \qquad (20)$$

First let us consider the case of longitudinally polarized K^*,

$$\frac{d\Gamma_L(B \to K^* \nu \bar{\nu})}{dq^2} = \frac{G_F^2 \alpha^2}{384 \pi^5} |C_L^V - C_R^V|^2 \frac{|p'|}{m_B^2 m_{K^*}^2}$$

$$\times [f(m_B E' - m_{K^*}^2) + 2 a_+ m_B^2 |p'|^2]^2, \qquad (21)$$

$$\frac{d\Gamma_L(B \to K^* \bar{\nu}\nu)}{dq^2} = \frac{G_F^2 \alpha^2}{256\pi^5} |C_L^S - C_R^S|^2 \frac{|p'|^3 q^2}{m_{K*}^2 (m_b + m_s)^2}$$

$$\times [f + a_+(m_B^2 - m_{K*}^2) + a_- q^2]^2$$

$$+ \frac{G_F^2 \alpha^2}{48\pi^5} |C_L^T|^2 \frac{|p'| q^2}{m_B^2 m_{K*}^2}$$

$$\times [g_+(m_B E' + m_{K*}^2)$$

$$+ g_-(m_B E' - m_{K*}^2) + 2h m_B^2 |p'|^2]^2, \tag{22}$$

$$\frac{d\Gamma_L(B \to K^* \nu\nu)}{dq^2} = \frac{G_F^2 \alpha^2}{256\pi^5} |\tilde{C}_L^S - \tilde{C}_R^S|^2 \frac{|p'|^3 q^2}{m_{K*}^2 (m_b + m_s)^2}$$

$$\times [f + a_+(m_B^2 - m_{K*}^2) + a_- q^2]^2$$

$$+ \frac{G_F^2 \alpha^2}{48\pi^5} |C_R^T|^2 \frac{|p'| q^2}{m_B^2 m_{K*}^2}$$

$$\times [g_+(m_B E' + m_{K*}^2)$$

$$+ g_-(m_B E' - m_{K*}^2) + 2h m_B^2 |p'|^2]^2. \tag{23}$$

The total differential decay rate, Eqs. (21)–(23), is given by

$$\frac{d\Gamma(B \to K^*)_L}{dq^2} \equiv \frac{d\Gamma(B \to K_{h=0}^*)}{dq^2} = |C_L^V - C_R^V|^2 V_L(q^2)$$

$$+ (|C_L^S - C_R^S|^2 + |\tilde{C}_L^S - \tilde{C}_R^S|^2) S_L(q^2)$$

$$+ (|C_L^T|^2 + |C_R^T|^2) T_L(q^2), \tag{24}$$

where

$$V_L(q^2) = \frac{G_F^2 \alpha^2}{384\pi^5} \frac{|p'|}{m_B^2 m_{K*}^2} [f(m_B E' - m_{K*}^2) + 2a_+ m_B^2 |p'|^2]^2, \tag{25}$$

$$S_L(q^2) = \frac{G_F^2 \alpha^2}{256\pi^5} \frac{|p'|^3 q^2}{m_{K*}^2 (m_b + m_s)^2}$$

$$\times [f + a_+(m_B^2 - m_{K*}^2) + a_- q^2]^2, \tag{26}$$

$$T_L(q^2) = \frac{G_F^2 \alpha^2}{48\pi^5} \frac{|p'| q^2}{m_B^2 m_{K*}^2} [g_+(m_B E' + m_{K*}^2)$$

$$+ g_-(m_B E' - m_{K*}^2) + 2h m_B^2 |p'|^2]^2. \tag{27}$$

In Fig. 1(b), we show $V_L(q^2)$, $S_L(q^2)$, and $T_L(q^2)$, which correspond to the solid, dashed, and dotted line, respectively. For the large-recoil limit, i.e., $q^2 \to 0$, the spectrum is similar to that of the $B \to K$ case. Near the zero-recoil point, the

sharp rise of the spectrum for the vector- and tensor-type interactions is observed while the spectrum of the scalar-type interaction is suppressed.

Now we turn to the case of transversely polarized K^*. For this case, the vector- and tensor-type interactions contribute to the process:

$$\frac{d\Gamma_{(\pm)}(B \to K^* \nu\bar{\nu})}{dq^2}$$

$$= \frac{G_F^2 \alpha^2}{384\pi^5} \frac{|p'| q^2}{m_B^2}$$

$$\times |(C_L^V + C_R^V) 2g m_B |p'| \mp (C_L^V - C_R^V) f|^2, \tag{28}$$

$$\frac{d\Gamma_{(\pm)}(B \to K^* \bar{\nu}\nu)}{dq^2}$$

$$= \frac{G_F^2 \alpha^2}{48\pi^5} |C_L^T|^2 \frac{|p'|}{m_B^2} \{2g_+ m_B |p'|$$

$$\pm [g_+(m_B^2 - m_{K*}^2) + g_- q^2]\}^2, \tag{29}$$

$$\frac{d\Gamma_{(\pm)}(B \to K^* \nu\nu)}{dq^2}$$

$$= \frac{G_F^2 \alpha^2}{48\pi^5} |C_R^T|^2 \frac{|p'|}{m_B^2} \{2g_+ m_B |p'|$$

$$\pm [g_+(m_B^2 - m_{K*}^2) + g_- q^2)]\}^2, \tag{30}$$

where $|p'|$ and E' are the K^* three-momentum magnitude and energy in the B-meson rest frame.

The total differential decay rate, Eqs. (28)–(30), is given by

$$\frac{d\Gamma(B \to K^*)_+}{dq^2} \equiv \frac{d\Gamma(B \to K_{h=+1}^*)}{dq^2}$$

$$= |C_L^V|^2 V_1(q^2) + |C_R^V|^2 V_2(q^2)$$

$$+ \text{Re}(C_L^V C_R^{V*}) V_3(q^2)$$

$$+ (|C_L^T|^2 + |C_R^T|^2) T_+(q^2), \tag{31}$$

$$\frac{d\Gamma(B \to K^*)_-}{dq^2} \equiv \frac{d\Gamma(B \to K_{h=-1}^*)}{dq^2}$$

$$= |C_L^V|^2 V_2(q^2) + |C_R^V|^2 V_1(q^2)$$

$$+ \text{Re}(C_L^V C_R^{V*}) V_3(q^2)$$

$$+ (|C_L^T|^2 + |C_R^T|^2) T_-(q^2), \tag{32}$$

where

$$V_1(q^2) = \frac{G_F^2 \alpha^2}{384\pi^5} \frac{|p'| q^2}{m_B^2} (2g m_B |p'| - f)^2, \tag{33}$$

$$V_2(q^2) = \frac{G_F^2 \alpha^2}{384 \pi^5} \frac{|p'|q^2}{m_B^2} (2gm_B|p'| + f)^2, \tag{34}$$

$$V_3(q^2) = \frac{G_F^2 \alpha^2}{384 \pi^5} \frac{|p'|q^2}{m_B^2} 2(4g^2 m_B^2 |p'|^2 - f^2), \tag{35}$$

$$T_\pm(q^2) = \frac{G_F^2 \alpha^2}{48 \pi^5} \frac{|p'|}{m_B^2} \{2g_+ m_B |p'|$$
$$\pm [g_+(m_B^2 - m_{K*}^2) + g_- q^2]\}^2. \tag{36}$$

In Figs. 1(c) and (d), we show V_1, V_2, V_3, T_-, and T_+. $V_1(q^2)$, $V_2(q^2)$, $V_3(q^2)$, and $T_-(q^2)$ correspond to the solid, dashed, dotted, and dot-dashed line, respectively, in Fig. 1(c), and $T_+(q^2)$ corresponds to the solid line in Fig. 1(d).

Note that in real experiments we cannot be able to distinguish the transverse polarization $h=+1$ from $h=-1$ due to the nondetection of the two neutrinos. Therefore, we have to add two transverse polarizations

$$\frac{d\Gamma(B \to K^*)_T}{dq^2} \equiv \frac{d\Gamma(B \to K^*_{h=+1})}{dq^2} + \frac{d\Gamma(B \to K^*_{h=-1})}{dq^2}. \tag{37}$$

We note that Eq. (37) is symmetric under the interchange of the variables C_L and C_R. Thus, we cannot distinguish the interactions with the opposite chirality structure using the spectrum. This contrasts with Ref. [5], where the asymmetry between $B \to K^*_{h=+1}$ and $B \to K^*_{h=-1}$ is assumed to be experimentally observed, thus leading to the measurement of the C_L and C_R separately.

IV. EFFECT OF NEW INTERACTIONS

In order to show the sensitivity of the branching ratios to the new physics effects, we show the dependence of the branching ratios on each coefficient. For the numerical computation of the branching ratio, we assume that there are three flavors of neutrinos, $\nu_{e,\mu,\tau}$, and the interactions in Eq. (1) are universal and diagonal on the neutrino flavors, i.e., $C_{L,Rij} = C_{L,R}\delta_{ij}$ and $\widetilde{C}_{L,Rij} = \widetilde{C}_{L,R}\delta_{ij}$. Therefore, we multiply three for the $\nu\bar\nu$ final states and multiply six ($=3\times2$) for the $\nu\nu(\bar\nu\bar\nu)$ final states. (See the Appendix for the statistical factors of theoretically indistinguishable neutrinos.)

The dependence of the branching ratios $\mathcal{BR}(B \to K)$, $\mathcal{BR}(B \to K^*_{h=0})$, $\mathcal{BR}(B \to K^*_{h=+1}) + \mathcal{BR}(B \to K^*_{h=-1})$, and $\mathcal{BR}(B \to K^*_{h=+1}) + \mathcal{BR}(B \to K^*_{h=-1}) + \mathcal{BR}(B \to K^*_{h=0})$ on the coefficients C_X are shown in Figs. 2(a), 2(b), 2(c), and 2(d), respectively. Here, the dependence on $C_X = \widetilde{C}_L^V/C_L^V(\mathrm{SM})$, $C_R^V/C_L^V(\mathrm{SM})$, $C_L^S/C_L^V(\mathrm{SM})$, and $C_L^T/C_L^V(\mathrm{SM})$ are corresponds to the solid, dashed, dotted, and dot-dashed lines, respectively, where $\widetilde{C}_L^V \equiv C_L^V - C_L^V(\mathrm{SM})$. In order to calculate the branching fraction of each process, we use the averaged lifetime of $B^\pm$ and B^0 from Particle Data Book [10],
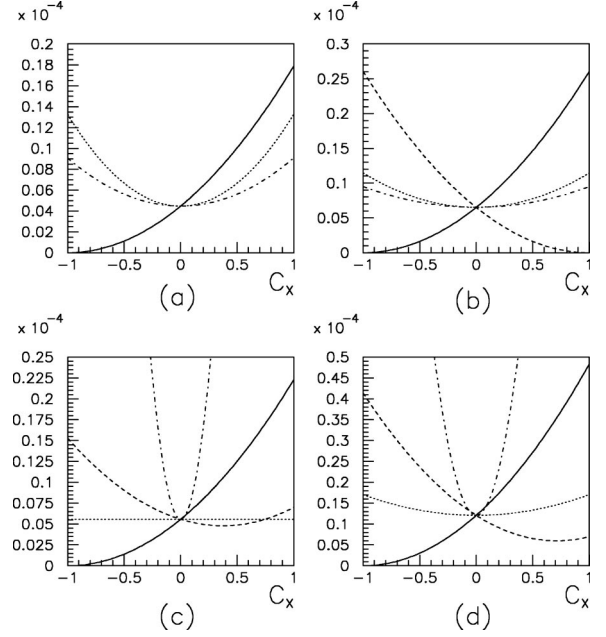

FIG. 2. The dependence of the branching ratios (a) $\mathcal{BR}(B \to K)$, (b) $\mathcal{BR}(B \to K^*)_L$, (c) $\mathcal{BR}(B \to K^*)_T$, and (d) $\mathcal{BR}(B \to K^*)$ on the coefficients C_X. The dependence on $C_X = \widetilde{C}_L^V/C_L^V(\mathrm{SM})$, $C_R^V/C_L^V(\mathrm{SM})$, $C_L^S/C_L^V(\mathrm{SM})$, and $C_L^T/C_L^V(\mathrm{SM})$ corresponds to the solid, dashed, dotted, and dot-dashed lines, respectively, where $\widetilde{C}_L^V \equiv C_L^V - C_L^V(\mathrm{SM})$.

$$\tau_{B^\pm} = (1.62 \pm 0.06) \times 10^{-12} \text{ sec}$$

and

$$\tau_{B^0} = (1.56 \pm 0.06) \times 10^{-12} \text{ sec}.$$

Figure 3 shows the dependence of the ratio R of produced K to K_T^* mesons, defined in Ref. [5] as

$$R \equiv \frac{\mathcal{BR}(B \to K)}{\mathcal{BR}(B \to K^*_{h=-1}) + \mathcal{BR}(B \to K^*_{h=+1})} \tag{38}$$

on the C_X, respectively. Here $C_X = \widetilde{C}_L^V/C_L^V(\mathrm{SM})$, $C_R^V/C_L^V(\mathrm{SM})$, $C_L^S/C_L^V(\mathrm{SM})$, and $C_L^T/C_L^V(\mathrm{SM})$, and the dependence on these coefficients corresponds to the solid, dashed, dotted, and dot-dashed lines, respectively.

In Figs. 4–7, we show the dependences of the differential branching ratios on the variation of (a) $C_X = \widetilde{C}_L^V/C_L^V(\mathrm{SM})$, (b) $C_R^V/C_L^V(\mathrm{SM})$, (c) $C_L^S/C_L^V(\mathrm{SM})$, and (d) $C_L^T/C_L^V(\mathrm{SM})$ for decays of $B \to K$ (Fig. 4), $B \to K^*_{h=0}$ (Fig. 5), $(B \to K^*_{h=+1}) + (B \to K^*_{h=-1})$ (Fig. 6), and $B \to K^*$ (Fig. 7). The thick solid line always indicates the SM case. In Fig. 4, the dependence of the differential branching ratios as a function of the missing mass squared is shown for $B \to K$ decay. In Fig. 4(a), the dashed, dotted, and dot-dashed lines correspond to $\widetilde{C}_L^V/C_L^V(\mathrm{SM}) = -0.7, 0.7, 1.0$ cases, respectively. In Fig. 4(b), the dashed, dotted, and dot-dashed lines correspond to $C_R^V/C_L^V(\mathrm{SM}) = -0.7, 0.7, 1.0$ cases, respectively. In Fig. 4(c), the dashed and dotted lines correspond to $C_L^S/C_L^V(\mathrm{SM}) = \pm 0.7, \pm 1.0$ cases, respectively. In Fig. 4(d), the dashed and
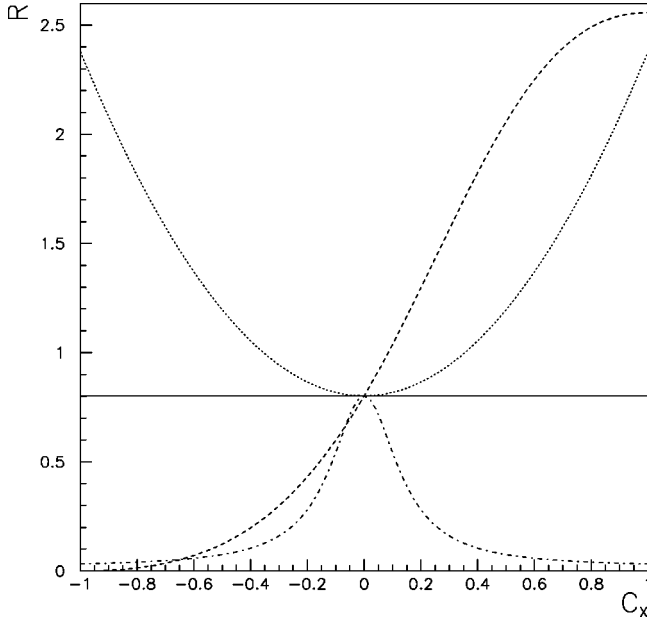
FIG. 3. The dependence of the ratio R [defined in Eq. (38)] on C_X. The dependence on $C_X = \tilde{C}_L^V/C_L^V(\text{SM})$, $C_R^V/C_L^V(\text{SM})$, $C_L^S/C_L^V(\text{SM})$, and $C_L^T/C_L^V(\text{SM})$ corresponds to the solid, dashed, dotted, and dot-dashed lines, respectively.

dotted lines correspond to $C_L^T/C_L^V(\text{SM}) = \pm 0.7, \pm 1.0$ cases, respectively. We can see that the vector-type interactions change the spectrum near the large-recoil limit ($q^2 \to 0$), while the scalar- and tensor-type interactions increase the spectrum in the center of the phase space and do not change the spectrum at the large-recoil limit.
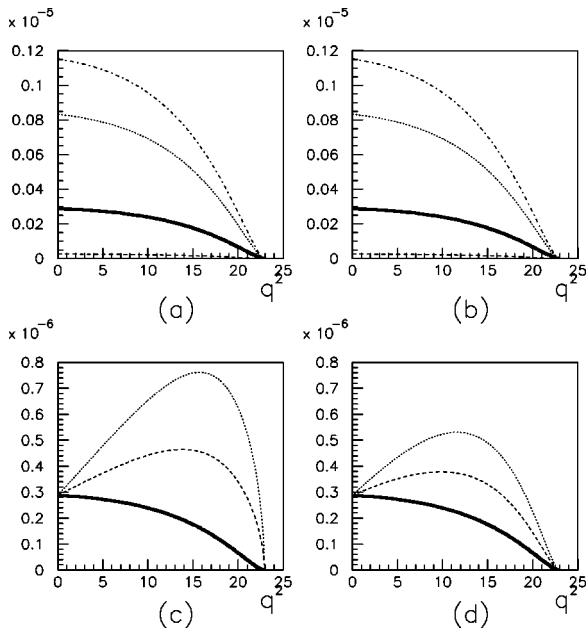
FIG. 4. The differential branching ratios for $(B \to K)$ depending on (a) $C_X = \tilde{C}_L^V/C_L^V(\text{SM})$, (b) $C_R^V/C_L^V(\text{SM})$, (c) $C_L^S/C_L^V(\text{SM})$, and (d) $C_L^T/C_L^V(\text{SM})$. The thick solid line indicates the SM case. See text for the numerical variation of C_X.
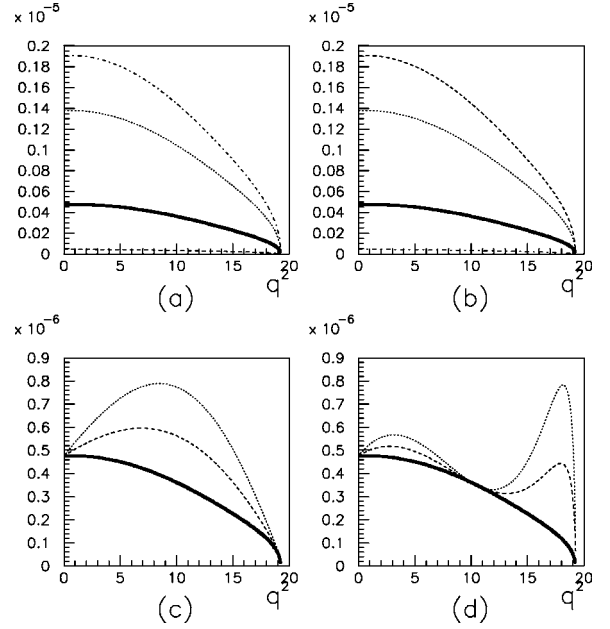

FIG. 5. The differential branching ratios for $(B \to K^*)_L$ as in Fig. 4.

In Fig. 5, the dependence of the differential branching ratios as a function of the missing mass squared is shown for $B \to K_{h=0}^*$ decays. In Fig. 5(a), the dashed, dotted, and dot-dashed lines correspond to $\tilde{C}_L^V/C_L^V(\text{SM}) = -0.7, 0.7, 1.0$ cases, respectively. In Fig. 5(b), the dashed, dotted, and dot-dashed lines correspond to $C_R^V/C_L^V(\text{SM}) = -1.0, -0.7, 0.7$ cases, respectively. In Fig. 5(c), the dashed and dotted line correspond to $C_L^S/C_L^V(\text{SM}) = \pm 0.7, \pm 1.0$ cases, respectively. In Fig. 5(d), the dashed and dotted lines correspond to $C_L^T/C_L^V(\text{SM}) = \pm 0.7, \pm 1.0$ cases, respectively. In this case
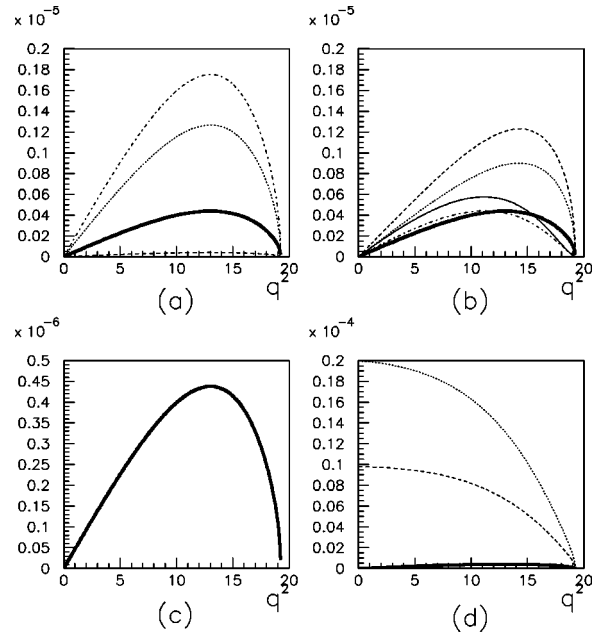

FIG. 6. The differential branching ratios for $(B \to K^*)_T$ as in Fig. 4.

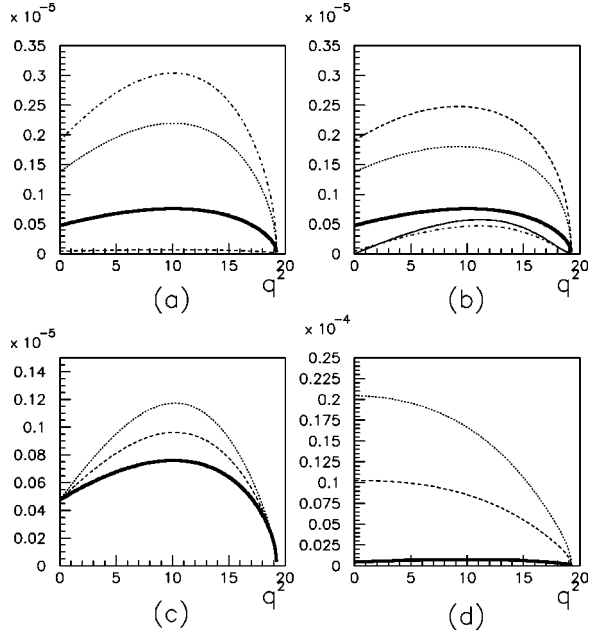FIG. 7. The differential branching ratios for $(B \to K^*)$ as in Fig. 4.

too, the vector-type interaction changes the spectrum for the large-recoil limit. However, the sign of the contribution of C_R is different from that of the $B \to K$ case [see Fig. 5(b)]. The scalar-type interaction enhances the spectrum at the center [see Fig. 5(c)] and the tensor-type interaction enhances the spectrum near the zero-recoil of K^* [see Fig. 5(d)].

In Fig. 6, the dependence of the differential branching ratios as a function of the missing mass squared for $(B \to K^*_{h=+1}) + (B \to K^*_{h=-1})$ decays is shown. In Fig. 6(a), the dashed, dotted, and dot-dashed lines correspond to $\widetilde{C}^V_L / C^V_L (\mathrm{SM}) = -0.7, 0.7, 1.0$ cases, respectively. In Fig. 6(b), the dashed, dotted, dot-dashed, and solid lines correspond to $C^V_R / C^V_L (\mathrm{SM}) = -1.0, -0.7, 0.7, 1.0$ cases, respectively. Figure 6(c) shows that there is no dependence on the C^S_L. In Fig. 6(d), the dashed and dotted lines correspond to $C^T_L / C^V_L (\mathrm{SM}) = \pm 0.7, \pm 1.0$ cases, respectively.

In Fig. 7, the dependence of the differential branching ratios as a function of the missing mass squared for $B \to K^*$ decays is shown, i.e., the sum of Figs. 5 and 6. In Fig. 7(a), the dashed, dotted, and dot-dashed lines correspond to $\widetilde{C}^V_L / C^V_L (\mathrm{SM}) = -0.7, 0.7, 1.0$ cases, respectively. In Fig. 7(b), the dashed, dotted, dot-dashed, and solid lines correspond to $C^V_R / C^V_L (\mathrm{SM}) = -1.0, -0.7, 0.7, 1.0$ cases, respectively. In Fig. 7(c), the dashed and dotted lines correspond to $C^S_L / C^V_L (\mathrm{SM}) = \pm 0.7, \pm 1.0$ cases, respectively. In Fig. 7(d), the dashed and dotted lines correspond to $C^T_L / C^V_L (\mathrm{SM}) = \pm 0.7, \pm 1.0$ cases, respectively. As one can see from the Figs. 4–7, the various new physics interactions have their own characteristic nature for the missing mass-squared spectrum. Therefore, these spectra can be used to discriminate the various new physics effects.

To summarize, we presented the possible new physics effects on $B \to K^{(*)} \nu \nu$ decays in a model-independent way.

With dimension-6 four-fermi interactions, not only the $B \to K^{(*)} \nu \bar{\nu}$ decay but also the total lepton-number-violating $B \to K^{(*)} \nu \nu$ or $B \to K^{(*)} \bar{\nu} \bar{\nu}$ decay may occur. Using the form factor of Ref. [8], we have shown how the branching ratios and the missing mass-squared spectrum depend on the new interactions. We can infer from the Figures that the branching ratios and the spectrum are useful for discriminating the various new physics effects systematically.

APPENDIX: STATISTICAL FACTORS FOR THEORETICALLY INDISTINGUISHABLE NEUTRINOS

We derive the relative statistical factors for the decay $B \to K \bar{\nu}_i \bar{\nu}_j (\nu_i \nu_j)$ for the case of the (theoretically) indistinguishable neutrinos $i = j$ as compared to the case of the (theoretically) distinguishable neutrinos $i \neq j$ (and $\nu \bar{\nu}$). First we define the neutrino field as

$$\psi_L = \sum_p \left[a_p u_{Lp} \exp(-ipx) + b_p^\dagger u_{Lp} \exp(ipx) \right], \quad \text{(A1)}$$

where u_{Lp} is four-component spinor which has only the lowest two components (η_p) nonzero: $u_{Lp} = (0, \eta_p)^T$. By defining the final two antineutrino states as $|p1^i, p2^j\rangle = b_{p1}^{i\dagger} b_{p2}^{j\dagger} |0\rangle$, we obtain

$$\langle p1^i, p2^j | \overline{\psi^C_{Li}} \psi_{Lj} |0\rangle = -i \delta_{ij} u_{Lj}(p2)^t \gamma_2 \gamma_0 u_{Li}(p1)$$
$$+ i u_{Li}(p1)^t \gamma_2 \gamma_0 u_{Lj}(p2) \quad \text{(A2)}$$

$$= i(1 + \delta_{ij}) u_{Li}(p1)^t \gamma_2 \gamma_0 u_{Lj}(p2). \quad \text{(A3)}$$

We can see that the matrix element for the indistinguishable neutrinos is enhanced by a factor of 2 (and, therefore, a factor of 4 for the amplitude squared) compared with the matrix element for the distinguishable case. After including a factor $1/2$ from the indistinguishable phase space, the decay rate for the indistinguishable neutrinos is twice larger than that of the distinguishable neutrinos. Even though experimentally all the neutrinos are practically indistinguishable in those environments, this factor two applies only to the theoretically indistinguishable case, i.e., $B \to K^{(*)} \nu_i \nu_i$ and $B \to K^{(*)} \bar{\nu}_i \bar{\nu}_i$.

[1] G. Buchalla and A. Buras, Nucl. Phys. **B400**, 225 (1993); Phys. Rev. D **54**, 6782 (1996).

[2] Y. Grossman and Y. Nir, Phys. Lett. B **398**, 163 (1997).

[3] Y. Grossman, Z. Ligeti, and E. Nardi, Nucl. Phys. **B465**, 369 (1996); **B480**, 753(E) (1996).

[4] T. M. Aliev and C. S. Kim, Phys. Rev. D **58**, 013003 (1998).

[5] D. Melikov, N. Nikitin, and S. Simula, Phys. Lett. B **428**, 171 (1998).

[6] S. Fukae, C. S. Kim, T. Morozumi, and T. Yoshikawa, Phys. Rev. D **59**, 074013 (1999).

[7] Y. Kiyo, T. Morozumi, P. Parada, M. N. Rebelo, and M. Tanimoto, Prog. Theor. Phys. **101**, 671 (1999).

[8] D. Melikhov, N. Nikitin, and S. Simula, Phys. Rev. D **57**, 6814 (1998).

[9] S. Godfrey and N. Isgur, Phys. Rev. D **32**, 189 (1985).

[10] Particle Data Group, C. Caso *et al.*, Eur. Phys. J. C **3**, 1 (1998).